Available online at www.sciencedirect.com
SCIENCE DIRECT®
Comput. Methods Appl. Mech. Engrg. 194 (2005) 4006–4023
Computer methods in applied mechanics and engineering
www.elsevier.com/locate/cma

Detection of cavities in Helmholtz-type equations using the boundary element method

Liviu Marin *

School of Earth and Environment, University of Leeds, Leeds LS2 9JT, UK

Received 26 May 2004; received in revised form 22 September 2004; accepted 19 October 2004

Abstract

Helmholtz-type equations arise naturally in many physical applications related to wave propagation, vibration phenomena and heat transfer. These equations are often used to describe the vibration of a structure, the acoustic cavity problem, the radiation wave, the scattering of a wave and heat conduction in fins. In this paper, the numerical recovery of a single and two circular cavities in Helmholtz-type equations from boundary data is investigated. The boundary element method (BEM), in conjunction with a constrained least-squares minimisation, is used to solve this inverse geometric problem. The accuracy and stability of the proposed numerical method with respect to the distance between the cavities and the outer boundary of the solution domain, the location and size of the cavities, and the distance between the cavities are also analysed. Unique and stable numerical solutions are obtained.

Keywords: Helmholtz-type equations; Inverse problem; Cavity detection; Boundary element method (BEM); Constrained minimisation

1. Introduction

A *direct problem* in the mathematical modelling of physical systems is to determine the response of a system, provided that the governing partial differential equations, the geometry of the domain of interest, the complete boundary and initial conditions, the material properties and the external sources acting in the solution domain are given, see e.g. [1]. When one or more of the conditions for solving the direct problem are partially or entirely unknown then an *inverse problem* may be formulated to determine the unknowns

* Tel.: +44 113 343 6744; fax: +44 113 343 6716.
E-mail address: liviu@env.leeds.ac.uk

0045-7825/$ - see front matter
doi:10.1016/j.cma.2004.10.005

from specified or measured system responses. It should be noted that most of the inverse problems are ill-posed and hence they are more difficult to solve than direct problems. It is well known that inverse problems are in general unstable, see e.g. Hadamard [2], in the sense that small measurement errors in the input data may amplify significantly the errors in the solution. In recent years, inverse problems have been extensively treated in several branches of science, such as solid mechanics [1], heat transfer [3], acoustic and electromagnetic scattering [4], electrical impedance tomography [5], etc. The most common approach is to determine the optimal estimates of the model parameters by minimising a selected measure-to-fit between the responses of the system and the model.

An important class of inverse problems in engineering consists of defects. Ikehata [5] has considered theoretically the reconstruction of polygonal cavities in two-dimensional domains, where the Laplace equation is satisfied from Cauchy data, whilst based on the previous method, Ikehata and Ohe [6] have numerically detected cavities from boundary measurements only. Tanaka and Masuda [7] have studied the retrieval of flaws or defects in structural components using the strains and the stresses as the reference data. The identification of an internal cavity equivalent to a single defect and plural defects in a structural component from the knowledge of the boundary conditions and some internal displacement measurements has been investigated by Tanaka et al. [8,9]. Bezerra and Saigal [10] have proposed a regularized boundary integral formulation for the detection of flaws in planar structural members from the displacement measurements given at some boundary locations and the applied loading. Nondestructive detection of internal cavity geometries in the inverse elastostatic problem has been studied by Mellings and Aliabadi [11], Kassab et al. [12] and Ulrich et al. [13]. Mallardo and Aliabadi [14] have identified a single elliptic cavity embedded in structures immersed in an inviscid fluid and illuminated by harmonic incident plane waves using the boundary element method (BEM), in conjunction with a first-order, non-linear, unconstrained optimisation technique. A study of the optimisation algorithms employed in identification inverse problems has been performed by Rus and Gallego [15], whilst later, they have detected both cracks and cavities using the the topological boundary integral method [16]. The simultaneous identification of the material constants and cavities embedded in an isotropic linear elastic medium has been undertaken by Marin et al. [17]. Recently, Divo et al. [18] and Kassab et al. [19] have presented an efficient solution of the inverse geometric problem of detection of subsurface cavities and flaws in two- and three-dimensions, respectively, by employing thermographic techniques.

Helmholtz-type equations arise naturally in many physical applications related to wave propagation, vibration phenomena and heat transfer. These equations are often used to describe the vibration of a structure [20], the acoustic cavity problem [21], the radiation wave [22], the scattering of a wave [23], acoustic scattering in fluid–solid problems [24] and the heat conduction in fins [25] and in the sequel, for the sake of physical meaning, we will refer to the later problem. We consider the inverse geometric problem to recover numerically circular cavities in Helmholtz-type equations from a single boundary measurement. Referring to heat conduction applications, the problem investigated in this study consists of determining a single and two circular cavities in the solution domain from a single boundary measurement of the temperature and heat flux. In this study, we propose a straightforward BEM to discretise the inverse problem under consideration. The BEM is further combined with a constrained least-squares minimisation routine. The accuracy and stability of the proposed numerical method with respect to the distance between the cavities and the outer boundary of the solution domain, the location and size of the cavities, and the distance between the cavities are also analysed.

2. Mathematical model

Referring to heat transfer for the sake of the physical explanation, we assume that the temperature field $T(\underline{x})$ satisfies the Helmholtz-type equation in a bounded domain $\Omega \subset \mathbb{R}^d$ (d is the dimension of the space in

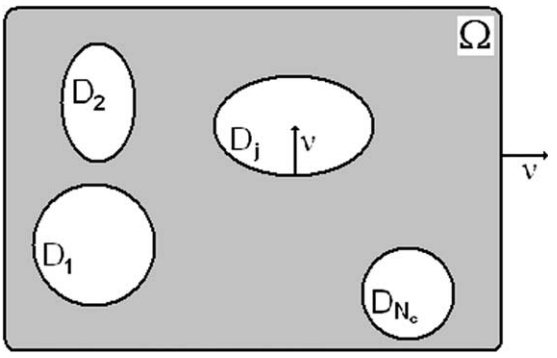

Fig. 1. A schematic diagram of the domain Ω and the cavities $\Omega_i = \bigcup_{j=1}^{N_c} D_j$.

which the problem is posed) containing N_c simply connected cavities D_j, $j = 1, \ldots, N_c$, with $\Omega_i \equiv \bigcup_{j=1}^{N_c} D_j \subset \Omega$ and $\overline{D}_j \cap \overline{D}_l = \emptyset$, $1 \leqslant j < l \leqslant N_c$, see Fig. 1, namely

$$\mathscr{L}T(\underline{x}) \equiv (\Delta + k^2)T(\underline{x}) = 0, \quad \underline{x} \in \Omega \setminus \overline{\Omega}_i, \tag{1}$$

where $k = \alpha + \mathrm{i}\beta$, $\mathrm{i} = \sqrt{-1}$, $\alpha, \beta \in \mathbb{R}$, and either $k \in \mathbb{R}$ (Helmholtz equation) or $k \in \mathbb{C} \setminus \mathbb{R}$ (modified Helmholtz equation). Additionally, we assume that the outer and inner boundaries $\partial\Omega$ and $\partial\Omega_i \equiv \bigcup_{j=1}^{N_c} \partial D_j$, respectively, are smooth enough such that Green's formula is applicable [26].

The general equation describing the temperature distribution along an isolated fin for steady state two-dimensional heat transfer is obtained by completing a heat balance over an incremental surface element, $\mathrm{d}\underline{y} = (y_1 - \mathrm{d}y_1/2, y_1 + \mathrm{d}y_1/2) \times (y_2 - \mathrm{d}y_2/2, y_2 + \mathrm{d}y_2/2)$, at some point, $\underline{y} = (y_1, y_2)$ within the fin surface, see e.g. [25]. The heat balance over the increment, $\mathrm{d}\underline{y}$, for steady state heat flow is given by

$$\begin{aligned}&(\dot{Q}_\mathrm{f}(y_1 - \mathrm{d}y_1/2, y_2) - \dot{Q}_\mathrm{f}(y_1 + \mathrm{d}y_1/2, y_2))\mathrm{d}y_2 \\ &\quad + (\dot{Q}_\mathrm{f}(y_1, y_2 - \mathrm{d}y_2/2) - \dot{Q}_\mathrm{f}(y_1, y_2 + \mathrm{d}y_2/2))\mathrm{d}y_1 - \dot{Q}_c(y_1, y_2) = 0,\end{aligned} \tag{2}$$

where $\dot{Q}_\mathrm{f}(y_1, y_2)$ is the conductive heat flow at $\underline{y} = (y_1, y_2)$ and $\dot{Q}_c(y_1, y_2)$ is the heat lost from the incremental surface of the fin. From the Postulation of Fourier, we have

$$\dot{Q}_\mathrm{f}(y_1, y_2) = -\lambda_\mathrm{f} A_\mathrm{f} \nabla\theta_\mathrm{f}(y_1, y_2), \tag{3}$$

where λ_f is the thermal conductivity of the fin and A_f is the cross-sectional area of the fin, and by using a Taylor series expansion around $\underline{y} = (y_1, y_2)$ and neglecting terms after the first-order derivatives we obtain

$$\begin{aligned}&(\dot{Q}_\mathrm{f}(y_1 - \mathrm{d}y_1/2, y_2) - \dot{Q}_\mathrm{f}(y_1 + \mathrm{d}y_1/2, y_2))\mathrm{d}y_2 + (\dot{Q}_\mathrm{f}(y_1, y_2 - \mathrm{d}y_2/2) - \dot{Q}_\mathrm{f}(y_1, y_2 + \mathrm{d}y_2/2))\mathrm{d}y_1 \\ &\quad = \nabla \cdot (\lambda_\mathrm{f} A_\mathrm{f} \nabla\theta_\mathrm{f}(y_1, y_2))\mathrm{d}y_1 \mathrm{d}y_2.\end{aligned} \tag{4}$$

The heat lost from the surface of the incremental fin is assumed to be by convection and, by Newton's law of cooling, this is given by

$$\dot{Q}_c(y_1, y_2) = hA'_\mathrm{f}(\theta_\mathrm{f}(y_1, y_2) - \theta_\infty)\mathrm{d}y_1\,\mathrm{d}y_2, \tag{5}$$

where h is the surface heat transfer coefficient, A'_f is the surface area of the fin per unit length and θ_∞ is the temperature of the surrounding medium.

Substitution of Eqs. (4) and (5) into the heat balance equation (2) provides the following second-order partial differential equation:

$$\nabla \cdot (\lambda_\mathrm{f} A_\mathrm{f} \nabla\theta_\mathrm{f}(\underline{y})) - hA'_\mathrm{f}(\theta_\mathrm{f}(\underline{y}) - \theta_\infty) = 0. \tag{6}$$

The following assumptions are invoked in order to obtain the general fin equation:

(i) The thermal conductivity of the fin, λ_f, is invariant.
(ii) The surface heat transfer coefficient, h, is uniform along the fin.
(iii) The temperature of the surrounding medium, θ_∞, is constant.

Additionally, if we assume that the cross-sectional area of the fin is constant (i.e. the fin thickness, $2\delta_f$, is invariant) then the fin equation (6) recasts as

$$\Delta\theta_f(\underline{y}) - \frac{h}{\lambda_f \delta_f}(\theta_f(\underline{y}) - \theta_\infty) = 0. \tag{7}$$

On introducing the following dimensionless variables:

$$x_j = y_j/\delta_f, \quad j = 1, 2, \qquad T(\underline{x}) = (\theta_f(\underline{y}) - \theta_\infty)/(\theta_b - \theta_\infty), \tag{8}$$

where θ_b is the fin base temperature ($\theta_b \neq \theta_\infty$), then the non-dimensional temperature distribution along an isolated fin of constant cross-sectional area for steady state two-dimensional heat transfer is described by the Helmholtz-type equation (1) with $k = \alpha + i\beta$, $\alpha = 0$ and $\beta = \sqrt{h/(\lambda_f \delta_f)}$.

We now let $v(\underline{x})$ be the outward normal vector at the boundary $\partial(\Omega \setminus \overline{\Omega}_i) \equiv \partial\Omega \cup \partial\Omega_i$ and $\Phi(\underline{x}) \equiv (\partial T/\partial v)(\underline{x})$ be the flux at a point $\underline{x} \in \partial(\Omega \setminus \overline{\Omega}_i)$. In the direct problem formulation, the knowledge of the location, shape and size of the cavities D_j, $j = 1, \ldots, N_c$, the temperature or the flux on the entire boundary, the temperature on the outer boundary and the flux on the inner boundary, or the flux on the outer boundary and the temperature on the inner boundary, gives the corresponding Dirichlet, Neumann or mixed boundary value problems, respectively, which enable us to determine the temperature $T(\underline{x})$ in the solution domain $\Omega \setminus \overline{\Omega}_i$. A more interesting situation occurs when the location, shape and size of the cavities D_j, $j = 1, \ldots, N_c$, are unknown and some additional information is supplied. More specifically, we analyse the following two problems.

Problem 1. Given $\widetilde{T} \in H^{1/2}(\partial(\Omega \setminus \overline{\Omega}_i))$ and $\widetilde{\Phi} \in H^{-1/2}(\partial\Omega)$, find the solution $(T, D_j; j = 1, \ldots, N_c)$ satisfying equation (1) when the temperature is known on the entire boundary $\partial(\Omega \setminus \overline{\Omega}_i)$, whilst flux measurements are available on the outer boundary $\partial\Omega$, namely

$$T(\underline{x}) = \widetilde{T}(\underline{x}), \quad \underline{x} \in \partial(\Omega \setminus \overline{\Omega}_i) \qquad \text{and} \qquad \Phi(\underline{x}) = \widetilde{\Phi}(\underline{x}), \quad \underline{x} \in \partial\Omega. \tag{9}$$

Problem 2. Given $\widetilde{T} \in H^{1/2}(\partial\Omega)$ and $\widetilde{\Phi} \in H^{-1/2}(\partial(\Omega \setminus \overline{\Omega}_i))$, find the solution $(T, D_j; j = 1, \ldots, N_c)$ satisfying Eq. (1) when the flux is known on the entire boundary $\partial(\Omega \setminus \overline{\Omega}_i)$, whilst temperature measurements are available on the outer boundary $\partial\Omega$, namely

$$\Phi(\underline{x}) = \widetilde{\Phi}(\underline{x}), \quad \underline{x} \in \partial(\Omega \setminus \overline{\Omega}_i) \quad \text{and} \quad T(\underline{x}) = \widetilde{T}(\underline{x}), \quad \underline{x} \in \partial\Omega. \tag{10}$$

In this study, we propose a straightforward BEM, as explained in the next section, to discretise the inverse problem given by Eqs. (1) and either (9) or (10). The BEM is further combined with a constrained least-squares minimisation routine. No regularization is required since we only look for the location and the size of *circular cavities* D_j, $j = 1, \ldots, N_c$, for which the uniqueness and stability hold, see e.g. [27] and [28], respectively.

3. Boundary element method

Let E_H and E_{MH} be the fundamental solutions of the Helmholtz and the modified Helmholtz equations, respectively, which in two-dimensions (i.e. $d = 2$) are given by, see e.g. [29]

$$E_{\mathrm{H}}(\underline{x},\underline{y}) = \frac{\mathrm{i}}{4}H_0^{(1)}(k|\underline{x}-\underline{y}|), \qquad E_{\mathrm{MH}}(\underline{x},\underline{y}) = \frac{1}{2\pi}K_0(k|\underline{x}-\underline{y}|), \tag{11}$$

where $H_0^{(1)}$ is the Hankel function of the first kind of order zero, K_0 is the modified Bessel function of the second kind of order zero and $\underline{x},\underline{y} \in \mathbb{R}^2$. The Helmholtz-type equation (1) can also be formulated in integral form [29] as

$$c(\underline{x})T(\underline{x}) + \int_{\Gamma}\frac{\partial E(\underline{x},\underline{y})}{\partial v(\underline{y})}T(\underline{y})\,\mathrm{d}\Gamma(\underline{y}) = \int_{\Gamma}E(\underline{x},\underline{y})\Phi(\underline{y})\,\mathrm{d}\Gamma(\underline{y}), \quad \underline{x} \in (\Omega\setminus\overline{\Omega}_i)\cup\partial(\Omega\setminus\overline{\Omega}_i), \tag{12}$$

where the first integral is taken in the sense of the Cauchy principal value, $c(\underline{x}) = 1$ for $\underline{x} \in \Omega\setminus\overline{\Omega}_i$ and $c(\underline{x}) = 1/2$ for $\underline{x} \in \partial(\Omega\setminus\overline{\Omega}_i)$ (smooth), and $E = E_{\mathrm{H}}$ or $E = E_{\mathrm{MH}}$.

Following a classical BEM, see [30,31], the outer boundary $\partial\Omega$ of the solution domain $\Omega\setminus\overline{\Omega}_i$ is discretised in an anti-clockwise direction into N_0 constant boundary elements $\Gamma_0^{(n)} = [\underline{y}^{(n-1)},\underline{y}^{(n)}]$, $n = 1,\ldots,N_0$, having the midpoints/collocation points $\underline{x}^{(n)} = (x_1^{(n)},x_2^{(n)})$, where $\underline{x}^{(n)} = (\underline{y}^{(n-1)} + \underline{y}^{(n)})/2$, $n = 1,\ldots,N_0$, and $\underline{y}^{(0)} \equiv \underline{y}^{(N_0)}$. For simplicity, we restrict ourselves to the detection of circular cavities $D_j = \{\underline{x} = (x_1,x_2)|(x_1-\eta_1^{(j)})^2 + (x_2-\eta_2^{(j)})^2 < r_j^2\}$, $j = 1,\ldots,N_c$, whilst the location and size of each cavity D_j, $j = 1,\ldots,N_c$, are completely determined by its centre $\underline{\eta}^{(j)} = (\eta_1^{(j)},\eta_2^{(j)})$ and radius r_j, $j = 1,\ldots,N_c$, respectively. Hence each unknown boundary (cavity) ∂D_j, $j = 1,\ldots,N_c$, is discretised in a clockwise sense into $N_i^{(j)}$ constant boundary elements $\Gamma_i^{(j,n)} = [\underline{y}^{(j,n-1)},\underline{y}^{(j,n)}]$, $n = 1,\ldots,N_i^{(j)}$, $j = 1,\ldots,N_c$, having the midpoints/collocation points $\underline{x}^{(j,n)} = (x_1^{(j,n)},x_2^{(j,n)})$, where $\underline{x}^{(j,n)} = (\underline{y}^{(j,n-1)} + \underline{y}^{(j,n)})/2$, $n = 1,\ldots,N_i^{(j)}$, $j = 1,\ldots,N_c$ and $\underline{y}^{(j,0)} \equiv \underline{y}^{(j,N_i^{(j)})}$, $j = 1,\ldots,N_c$. Furthermore, for every $j = 1,\ldots,N_c$ the coordinates of the boundary points $\underline{y}^{(j,n)} = (y_1^{(j,n)},y_2^{(j,n)})$, $n = 0,\ldots,N_i^{(j)}$, and the collocation points $\underline{x}^{(j,n)} = (x_1^{(j,n)},x_2^{(j,n)})$, $n = 1,\ldots,N_i^{(j)}$, can be expressed with respect to the coordinates of the centre $\underline{\eta}^{(j)} = (\eta_1^{(j)},\eta_2^{(j)})$ and the radius r_j of the corresponding unknown cavity D_j, namely

$$y_1^{(j,n)} = \eta_1^{(j)} + r_j\cos(2n\pi/N_i^{(j)}), \qquad y_2^{(j,n)} = \eta_2^{(j)} + r_j\sin(2n\pi/N_i^{(j)}), \quad n = 0,\ldots,N_i^{(j)} \tag{13}$$

and

$$\begin{cases} x_1^{(j,n)} = \eta_1^{(j)} + (r_j/2)\{\cos(2n\pi/N_i^{(j)}) + \cos(2(n-1)\pi/N_i^{(j)})\}, & n = 1,\ldots,N_i^{(j)} \\ x_2^{(j,n)} = \eta_2^{(j)} + (r_j/2)\{\sin(2n\pi/N_i^{(j)}) + \sin(2(n-1)\pi/N_i^{(j)})\}, & n = 1,\ldots,N_i^{(j)}. \end{cases} \tag{14}$$

Let us make the following notation:

$$\begin{aligned} &\Gamma_n = \Gamma_0^{(n)}, && \underline{z}^{(n)} = \underline{x}^{(n)}, && n = 1,\ldots,N_0 \\ &\Gamma_{N_0+\sum_{m=1}^{j}N_i^{(m)}+n} = \Gamma_i^{(j,n)}, && \underline{z}^{\left(N_0+\sum_{m=1}^{j}N_i^{(m)}+n\right)} = \underline{x}^{(j,n)}, && n = 1,\ldots,N_i^{(j)}, \quad j = 1,\ldots,N_c \\ &T_n = T(\underline{z}^{(n)}), && \Phi_n = \Phi(\underline{z}^{(n)}), && n = 1,\ldots,N \end{aligned} \tag{15}$$

where $N = N_0 + N_i$ and $N_i = \sum_{j=1}^{N_c}N_i^{(j)}$. On approximating the temperature and the flux on the boundary $\partial(\Omega\setminus\overline{\Omega}_i)$ by piecewise constant functions over each boundary element Γ_n, $n = 1,\ldots,N$, namely their values T_n and Φ_n, respectively, at the collocation point $\underline{z}^{(n)} \in \Gamma_n$, then the discretised form of the boundary integral equation (12) can be written as

$$c(\underline{z})T(\underline{z}) + \sum_{n=1}^{N}A_n\left(\underline{z},\eta_1^{(j)},\eta_2^{(j)},r_j;j = 1,\ldots,N_c\right)T_n = \sum_{n=1}^{N}B_n\left(\underline{z},\eta_1^{(j)},\eta_2^{(j)},r_j;j = 1,\ldots,N_c\right)\Phi_n \tag{16}$$

for all $\underline{z} \in (\Omega\setminus\overline{\Omega}_i)\cup\partial(\Omega\setminus\overline{\Omega}_i)$, where

$$A_n\left(\underline{z},\eta_1^{(j)},\eta_2^{(j)},r_j;j=1,\ldots,N_c\right)=\int_{\Gamma_n}\frac{\partial E(\underline{z},\underline{y})}{\partial v(\underline{y})}\,\mathrm{d}\Gamma(\underline{y}),$$
$$B_n\left(\underline{z},\eta_1^{(j)},\eta_2^{(j)},r_j;j=1,\ldots,N_c\right)=\int_{\Gamma_n}E(\underline{z},\underline{y})\,\mathrm{d}\Gamma(\underline{y}). \tag{17}$$

By applying the discretised boundary integral equation (16) at each collocation point $\underline{z}^{(m)}$, $m=1,\ldots,N$, we arrive at the system of equations

$$\sum_{n=1}^{N}\left\{A_{mn}\left(\eta_1^{(j)},\eta_2^{(j)},r_j;j=1,\ldots,N_c\right)T_n-B_{mn}\left(\eta_1^{(j)},\eta_2^{(j)},r_j;j=1,\ldots,N_c\right)\Phi_n\right\}=0,\quad m=1,\ldots,N, \tag{18}$$

where the non-linear functions $A_{mn}(\eta_1^{(j)},\eta_2^{(j)},r_j;j=1,\ldots,N_c)$ and $B_{mn}(\eta_1^{(j)},\eta_2^{(j)},r_j;j=1,\ldots,N_c)$, $m,n=1,\ldots,N$, are given by

$$A_{mn}\left(\eta_1^{(j)},\eta_2^{(j)},r_j;j=1,\ldots,N_c\right)=A_n\left(\underline{z}^{(m)},\eta_1^{(j)},\eta_2^{(j)},r_j;j=1,\ldots,N_c\right)+\delta_{mn}/2,$$
$$B_{mn}\left(\eta_1^{(j)},\eta_2^{(j)},r_j;j=1,\ldots,N_c\right)=B_n\left(\underline{z}^{(m)},\eta_1^{(j)},\eta_2^{(j)},r_j;j=1,\ldots,N_c\right), \tag{19}$$

with δ_{mn} the Kronecker tensor.

4. Description of the algorithm

In the sequel we focus on Problem 1 given by Eqs. (1) and (9), with the mention that Problem 2 given by Eqs. (1) and (10) can be treated in a similar manner. If we consider the discretised BEM system (18) recast as the solution of a direct problem with the boundary conditions $\Phi(\underline{x})=\widetilde{\Phi}(\underline{x})$, $\underline{x}\in\partial\Omega$ and $T(\underline{x})=\widetilde{T}(\underline{x})$, $\underline{x}\in\partial\Omega_i$, namely

$$\begin{aligned}\sum_{n=1}^{N_0}A_{mn}(\eta_1^{(j)},\eta_2^{(j)},r_j;j=1,\ldots,N_c)T_n-\sum_{n=N_0+1}^{N}B_{mn}(\eta_1^{(j)},\eta_2^{(j)},r_j;j=1,\ldots,N_c)\Phi_n\\ =\sum_{n=1}^{N_0}B_{mn}(\eta_1^{(j)},\eta_2^{(j)},r_j;j=1,\ldots,N_c)\widetilde{\Phi}_n\\ -\sum_{n=N_0+1}^{N}A_{mn}(\eta_1^{(j)},\eta_2^{(j)},r_j;j=1,\ldots,N_c)\widetilde{T}_n,\quad m=1,\ldots,N,\end{aligned} \tag{20}$$

then the calculated temperatures T_n, $n,=1,\ldots,N_0$, on the outer boundary $\partial\Omega$ and fluxes Φ_n, $n=N_0+1,\ldots,N$, on the inner boundary $\partial\Omega_i$ are functions of the unknown parameters $\eta_1^{(j)}$, $\eta_2^{(j)}$ and r_j which determine the location and size of the cavities D_j, $j=1,\ldots,N_c$, i.e.

$$T_n=T_n(\eta_1^{(j)},\eta_2^{(j)},r_j;j=1,\ldots,N_c),\quad n=1,\ldots,N_0$$
$$\Phi_n=\Phi_n(\eta_1^{(j)},\eta_2^{(j)},r_j;j=1,\ldots,N_c),\quad n=N_0+1,\ldots,N. \tag{21}$$

The numerical scheme proposed in this study is based on the minimisation of the objective function

$$\mathscr{F}(\eta_1^{(j)},\eta_2^{(j)},r_j;j=1,\ldots,N_c)=\frac{1}{2}\sum_{n=1}^{N_0}\{T_n(\eta_1^{(j)},\eta_2^{(j)},r_j;j=1,\ldots,N_c)-\widetilde{T}_n\}^2, \tag{22}$$

subject to the physical constraints which require that the circular cavities D_j, $j=1,\ldots,N_c$, stay within the domain Ω ($\overline{D}_j\subset\Omega, j=1,\ldots,N_c$) and any two distinct cavities D_j and D_l, $1\leqslant j<l\leqslant N_c$, be disjointed

$(\overline{D}_j \cup \overline{D}_l = \emptyset, 1 \leqslant j < l \leqslant N_c)$. In the case of Problem 2, it should be noted that the discretised BEM system of equations (18) is regarded as the solution of a direct problem with the boundary conditions $T(\underline{x}) = \widetilde{T}(\underline{x})$, $\underline{x} \in \partial\Omega$ and $\Phi(\underline{x}) = \widetilde{\Phi}(\underline{x})$, $\underline{x} \in \partial\Omega_i$, whilst the objective function $\mathscr{F}$ minimises the difference between the calculated $\Phi_n(\eta_1^{(j)}, \eta_2^{(j)}, r_j; j = 1, \ldots, N_c)$, $n = 1, \ldots, N_0$, and the measured fluxes $\widetilde{\Phi}_n$, $n = 1, \ldots, N_0$, on the outer boundary $\partial\Omega$, namely

$$\mathscr{F}(\eta_1^{(j)}, \eta_2^{(j)}, r_j; j = 1, \ldots, N_c) = \frac{1}{2} \sum_{n=1}^{N_0} \{\Phi_n(\eta_1^{(j)}, \eta_2^{(j)}, r_j; j = 1, \ldots, N_c) - \widetilde{\Phi}_n\}^2. \tag{23}$$

If we assume that the domain Ω is a disk of radius R centred in the origin, i.e. $\Omega = \underline{x} = (x_1, x_2) \mid x_1^2 + x_2^2 < R^2\}$, then the following $3N_c$ physical bounds and N_c for $N_c = 1$ or $N_c(N_c - 1)/2$ for $N_c \geqslant 2$ nonlinear constraints, respectively, are imposed on the geometrical variables which determine the circular cavities D_j, $j = 1, \ldots, N_c$:

$$-R < \eta_1^{(j)} < R, \quad -R < \eta_2^{(j)} < R, \quad 0 < r_j < R, \quad j = 1, \ldots, N_c, \tag{24}$$

$$r_j + r_l < \sqrt{(\eta_1^{(j)} - \eta_1^{(l)})^2 + (\eta_2^{(j)} - \eta_2^{(l)})^2} < (R - r_j) + (R - r_l), \quad 1 \leqslant j < l \leqslant N_c. \tag{25}$$

It should be mentioned that the geometrical constraints (24) and (25) can be easily formulated provided that the domain Ω is simple, e.g. triangle, square, rectangle, hexagon, etc., however, it is more difficult to express these constraints for a domain with a general shape.

Numerically, the objective function (22) is minimised using the NAG subroutine E04UPF, which is designed to minimise an arbitrary smooth sum of squares subject to constraints. This may include simple bounds on the variables, linear constraints and smooth nonlinear constraints. Each iteration of the subroutine includes the following: (a) the solution of a quadratic programming subproblem; (b) a line search with an augmented Lagrangian function; and (c) a quasi-Newton update of the approximate Hessian of the Lagrangian function, for more details, see [32]. It should be noted that it is important to impose the constraints (24) and (25) in order to generate feasible solutions since unconstrained minimisation was found to produce physically meaningless solutions. The gradient of the objective function (22) has been calculated using forward finite differences with a step of 10^{-3} which was found to be sufficiently small that a further decrease in this value does not affect significantly the accuracy of the numerical results.

5. Numerical results and discussion

It should be mentioned that the numerical technique proposed in this study can be regarded as a particular case of the algorithm introduced by Mallardo and Aliabadi [14], in the sense that these authors detected a single elliptical cavity in the case when the scalar Helmholtz equation was coupled with the vectorial Cauchy–Navier equations. However, the retrieval of a single and two cavities embedded in a domain where Helmholtz-type equations are satisfied from boundary data can be attained accurately and stably using the simple constrained least-squares minimisation technique presented in Section 4, in conjunction with the BEM described in Section 3, as will be shown in this section.

In order to present the performance of the numerical method proposed, we solve the inverse geometric Problem 1 for both the Helmholtz and the modified Helmholtz equations by considering three examples in a two-dimensional smooth geometry, namely the disk

$$\Omega = \{\underline{x} = (x_1, x_2) | x_1^2 + x_2^2 < R^2\}, \quad R = 1.50, \tag{26}$$

in which a single and two circular cavities are embedded

$$\overline{\Omega}_i \subset \Omega: \quad \Omega_i = \bigcup_{j=1}^{N_c} D_j, \quad D_j = \{\underline{x} = (x_1, x_2) \,|\, (x_1 - \eta_1^{(j)})^2 + (x_2 - \eta_2^{(j)})^2 < r_j^2\}, \quad j = 1, \ldots, N_c, \tag{27}$$

where $N_c = 1$ and $N_c = 2$, respectively. Herein, we do not consider more cavities since theoretical results are not available as yet.

5.1. Examples

We consider the following analytical solutions for the temperature and its corresponding boundary flux associated with the Helmholtz-type operator, namely

(H) The Helmholtz equation ($k = \alpha + \mathrm{i}\beta$, $\alpha \in \mathbb{R}$, $\beta = 0$)

$$\begin{aligned} T^{(\mathrm{an})}(\underline{x}) &= \cos(a_1 x_1 + a_2 x_2), \quad \underline{x} = (x_1, x_2) \in \Omega \setminus \overline{\Omega}_i \\ \Phi^{(\mathrm{an})}(\underline{x}) &= -\sin(a_1 x_1 + a_2 x_2)(a_1 v_1(\underline{x}) + a_2 v_2(\underline{x})), \quad \underline{x} = (x_1, x_2) \in \partial(\Omega \setminus \overline{\Omega}_i), \end{aligned} \tag{28}$$

where $\alpha = 1.00$, $a_1 = 0.50$ and $a_2 = \sqrt{\alpha^2 - a_1^2}$.

(MH) The modified Helmholtz equation ($k = \alpha + \mathrm{i}\beta$, $\alpha = 0$, $\beta \in \mathbb{R}$)

$$\begin{aligned} T^{(\mathrm{an})}(\underline{x}) &= \exp(a_1 x_1 + a_2 x_2), \quad \underline{x} = (x_1, x_2) \in \Omega \setminus \overline{\Omega}_i \\ \Phi^{(\mathrm{an})}(\underline{x}) &= \exp(a_1 x_1 + a_2 x_2)(a_1 v_1(\underline{x}) + a_2 v_2(\underline{x})), \quad \underline{x} = (x_1, x_2) \in \partial(\Omega \setminus \overline{\Omega}_i), \end{aligned} \tag{29}$$

where $\beta = 1.00$, $a_1 = 0.50$ and $a_2 = \sqrt{\beta^2 - a_1^2}$.

In the sequel, we analyse the numerical method presented in Section 4, in conjunction with the BEM described in Section 3, by solving the Problem 1 for the following examples:

Example 1. The Helmholtz equation ($k = \alpha + \mathrm{i}\beta$, $\alpha \in \mathbb{R}$, $\beta = 0$) in the disk Ω given by (26) containing a single cavity, i.e. $N_c = 1$ in (27), and having the analytical solution (28).

Example 2. The modified Helmholtz equation ($k = \alpha + \mathrm{i}\beta$, $\alpha = 0$, $\beta \in \mathbb{R}$) in the disk Ω given by (26) containing a single cavity, i.e. $N_c = 1$ in (27), and having the analytical solution (29).

Example 3. The modified Helmholtz equation ($k = \alpha + \mathrm{i}\beta$, $\alpha = 0$, $\beta \in \mathbb{R}$) in the disk Ω given by (26) containing two cavities, i.e. $N_c = 2$ in (27), and having the analytical solution (29).

It is worth noting that by considering the analytical data (28) and (29) as input data in the inverse problem under consideration, we inherently introduce numerical noise. An alternative way to fabricate the input data for the inverse problem is to solve a direct problem with complete boundary conditions and consider the numerically retrieved boundary temperature or flux on $\partial\Omega$ as the input data for the inverse problem. More specifically, since analytical expressions for both the temperature and the flux are available in the domain $\Omega \setminus \overline{\Omega}_i$, we may solve the following mixed boundary value problem:

$$\begin{cases} \mathscr{L} T^{(\mathrm{ex})}(\underline{x}) = 0, & \underline{x} \in \Omega \setminus \overline{\Omega}_i \\ \Phi^{(\mathrm{ex})}(\underline{x}) = \Phi^{(\mathrm{an})}(\underline{x}), & \underline{x} \in \partial\Omega \\ T^{(\mathrm{ex})}(\underline{x}) = T^{(\mathrm{an})}(\underline{x}), & \underline{x} \in \partial\Omega_i \end{cases} \tag{30}$$

in order to obtain the numerical temperature $T^{(\mathrm{ex})}|_{\partial\Omega}$. Hence the inverse problem under investigation is given by Eqs. (1) and (9) in which the input boundary data $\widetilde{\Phi}|_{\partial\Omega} = \Phi^{(\mathrm{an})}|_{\partial\Omega}$ and $\widetilde{T}|_{\partial\Omega_i} = T^{(\mathrm{an})}|_{\partial\Omega_i}$ are given by the corresponding analytical expressions (28) or (29), whilst the input boundary data $\widetilde{T}|_{\partial\Omega} = T^{(\mathrm{ex})}|_{\partial\Omega}$

is obtained by solving numerically the mixed boundary value problem (30), and in what follows they will be referred to as "exact data".

The numerical results presented in this section have been obtained using a discretisation of the outer boundary $\partial\Omega$ and the inner boundary $\partial\Omega_i$ corresponding to the cavities D_j, $j = 1, \ldots, N_c$, with $N_0 = 20$ and $N_i = \sum_{j=1}^{N_c} N_i^{(j)}$ boundary elements, respectively, where $N_i^{(j)} = 20$, $j = 1, \ldots, N_c$, i.e. the total number of boundary elements used for the discretisation of the problem is given by $N = N_0 + N_i = 20(N_c + 1)$. These values were found to be sufficiently large such that any further refinement of the mesh size did not significantly improve the accuracy of the results.

5.2. Stability of the method

Exact data is seldom available in practice since measurement errors always include noise in the prescribed boundary conditions and this is studied next. In order to investigate the stability of the numerical method proposed, the boundary data $\widetilde{T}|_{\partial\Omega}$ has been perturbed as

$$\widetilde{T}^{\varepsilon}|_{\partial\Omega} = \widetilde{T}|_{\partial\Omega} + \delta\widetilde{T}, \quad \delta\widetilde{T} = \mathrm{G05DDF}(0, \sigma), \quad \sigma = \max_{\partial\Omega} |\widetilde{T}| \frac{p_T}{100}, \tag{31}$$

where $\delta\widetilde{T}$ is a Gaussian random variable with mean zero and standard deviation σ, generated by the NAG subroutine G05DDF, and p_T is the percentage of additive noise included in the input data $\widetilde{T}|_{\partial\Omega}$ in order to simulate the inherent measurement errors.

Starting with an arbitrary initial guess $(\eta_1^{(j,\mathrm{g})}, \eta_2^{(j,\mathrm{g})}, r_j^{(\mathrm{g})}; j = 1, \ldots, N_c)$, for the cavities $D_j, j = 1, \ldots, N_c$, we estimate their exact values, $(\eta_1^{(j)}, \eta_2^{(j)}, r_j; j = 1, \ldots, N_c)$, using the numerical method proposed in Section 4 and various levels of noise p_T added into the input temperature data $T|_{\partial\Omega}$, for the examples considered. More precisely, we consider the following exact solutions and initial guesses for the parameters describing the cavities:

(E1) D_1: $\eta_1^{(1)} = -0.20$, $\eta_2^{(1)} = -0.30$, $r_1 = 0.50$;

(E2) D_1: $\eta_1^{(1)} = 0.20$, $\eta_2^{(1)} = 0.30$, $r_1 = 0.70$;

(E3) D_1: $\eta_1^{(1)} = 0.70$, $\eta_2^{(1)} = 0.50$, $r_1 = 0.40$; D_2: $\eta_1^{(2)} = -0.60$, $\eta_2^{(2)} = -0.40$, $r_2 = 0.20$;

and

(G1) $D_1^{(\mathrm{g})}$: $\eta_1^{(1,\mathrm{g})} = \eta_2^{(1,\mathrm{g})} = 0.0$, $r_1^{(\mathrm{g})} = 1.40$;

(G2) $D_1^{(\mathrm{g})}$: $\eta_1^{(1,\mathrm{g})} = \eta_2^{(1,\mathrm{g})} = 0.0$, $r_1^{(\mathrm{g})} = 1.40$;

(G3) $D_1^{(\mathrm{g})}$: $\eta_1^{(1,\mathrm{g})} = 0.0$, $\eta_2^{(1,\mathrm{g})} = 0.70$, $r_1^{(\mathrm{g})} = 0.60$; $D_2^{(\mathrm{g})}$: $\eta_1^{(1,\mathrm{g})} = 0.0$, $\eta_2^{(1,\mathrm{g})} = -0.70$, $r_2^{(\mathrm{g})} = 0.60$;

for the numerical Examples 1–3 described in Section 5.1, respectively.

Fig. 2 illustrates the exact and the numerical solution for the cavity D_1 given by (E1), obtained for Example 1 starting with the initial guess (G1) and various levels of noise added into the input temperature $\widetilde{T}|_{\partial\Omega}$, namely $p_T \in \{1, 3, 5, 7, 10\}$. It can be seen that as p_T decreases, so the level of noise added into the input data $\widetilde{T}|_{\partial\Omega}$ also decreases, then the numerical solution for the cavity D_1 more closely approximates the exact target, while remaining at the same time stable. The same conclusion can be drawn from Table 1 which presents the values of the objective function $\mathscr{F}$, the number of iterations performed n_{iter}, the numerically retrieved values for the parameters characterising the position and the shape of the cavity D_1 and the corresponding percentage absolute errors defined by

$$\mathrm{Err}(\eta_i^{(j)}) = \frac{|\eta_i^{(j)} - \eta_i^{(j,\mathrm{num})}|}{|\eta_i^{(j)}|} \times 100, \quad \mathrm{Err}(r_j) = \frac{|r_j - r_j^{(\mathrm{num})}|}{|r_j|} \times 100, \quad i = 1, 2, \quad j = 1, \ldots, N_c, \tag{32}$$

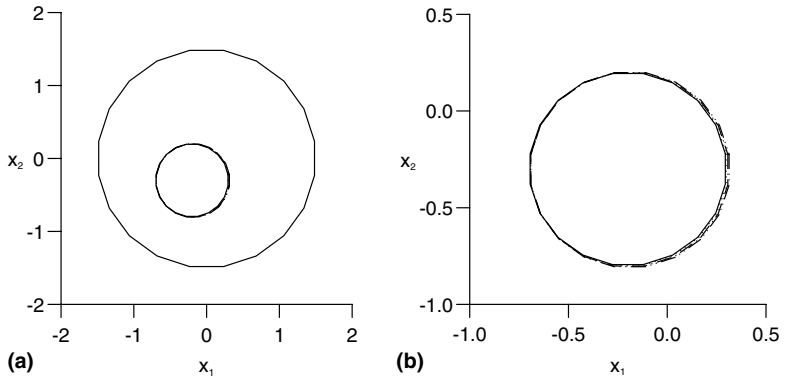

Fig. 2. (a) The exact (—) and the numerical solution for the cavity D_1 given by (E1), obtained with the initial guess (G1) and various levels of noise added into the temperature data $T|_{\partial\Omega}$, namely $p_T = 1\%$ (···), $p_T = 3\%$ (– · –), $p_T = 5\%$ (–···–), $p_T = 7\%$ (–····–) and $p_T = 10\%$ (–·····–), for Example 1, and (b) a closer view of the exact and numerical results obtained for the cavity D_1.

Table 1
The values of the objective function $\mathscr{F}$, the number of iterations performed n_{iter} and the numerically retrieved values for the parameters characterising the position and the shape of the cavity D_1 given by $\eta_1^{(1)} = -0.20$, $\eta_2^{(1)} = -0.30$ and $r_1 = 0.50$, obtained using the initial guess $\eta_1^{(1,g)} = \eta_2^{(1,g)} = 0.0$ and $r_1^{(g)} = 1.40$, and various levels p_T of noise added into the input temperature data $T^{(\text{an})}|_{\partial\Omega}$, for Example 1

p_T	$\eta_1^{(1,\text{num})}$	$\text{Err}(\eta_1^{(1)})$	$\eta_2^{(1,\text{num})}$	$\text{Err}(\eta_2^{(1)})$	$r_1^{(\text{num})}$	$\text{Err}(r_1)$	$\mathscr{F}$	n_{iter}
1	−0.1968	1.5903	−0.3013	0.4192	0.5016	0.3209	0.8206×10^{-8}	8
3	−0.1922	3.9000	−0.3028	0.9308	0.5048	0.9567	0.7671×10^{-7}	9
5	−0.1891	5.4542	−0.3035	1.1625	0.5079	1.5843	0.2217×10^{-6}	9
7	−0.1868	6.5766	−0.3036	1.1939	0.5110	2.2040	0.4521×10^{-6}	9
10	−0.1844	7.8031	−0.3037	1.2383	0.5156	3.1191	0.9779×10^{-6}	9

obtained with the noisy input data $\widetilde{T}^{\varepsilon}$ given by (31). It can be seen from this table that the objective function $\mathscr{F}$ decreases as the level of noise added into the outer boundary temperature data decreases and the number of iterations performed n_{iter} is relatively small.

The exact and numerical solutions for the cavities D_j, $j = 1, \ldots, N_c$, given by (E2) and (E3), obtained using various levels of noise added into the input temperature $\widetilde{T}|_{\partial\Omega}$ and the initial guess (G2) for Example 2 and (G3) for Example 3 are presented in Figs. 3 and 4, respectively. From Figs. 2(b) and 3(b), and Fig. 4(a) and (b), respectively, it can be noticed that cavities with a large radius are more accurately retrieved than cavities with a small radius. However, the numerical results obtained for the location and size of the cavities D_j, $j = 1, \ldots, N_c$, embedded in the domain Ω using the algorithm presented in Section 4 represent very good approximations for their exact values for all the examples analysed. Moreover, from Figs. 2–4 and Table 1 we can conclude that the proposed numerical method is stable with respect to decreasing the amount of noise added into the input data.

Fig. 5(a) and (b) illustrate the behaviour of the percentage absolute errors $\text{Err}(\eta_1^{(1)})$, $\text{Err}(\eta_2^{(1)})$ and $\text{Err}(r_1)$, defined by relations (32), obtained with $p_T = 10\%$ noise added into the input temperature $\widetilde{T}|_{\partial\Omega}$ and the initial guesses (G1) and (G2) for Examples 1 and 2, respectively, with respect to the number of iterations n_{iter} performed. From these figures it can be seen that the minimisation process is very rapid, in the sense that the errors given by (32) decrease very rapidly and attain reasonable values after a small number of iterations, namely $n_{\text{iter}} = 5$ and $n_{\text{iter}} = 7$ for Examples 1 and 2, respectively. Although not presented here, it should be noted that the evolution of the absolute errors $\text{Err}(\eta_1^{(j)})$, $\text{Err}(\eta_2^{(j)})$ and $\text{Err}(r_j)$, $j = 1, 2$, obtained using the initial guess (G3) and noisy input temperature data $\widetilde{T}|_{\partial\Omega}$ for Example 3, is similar to that presented in Fig. 5(a) and (b) for Examples 1 and 2, respectively.

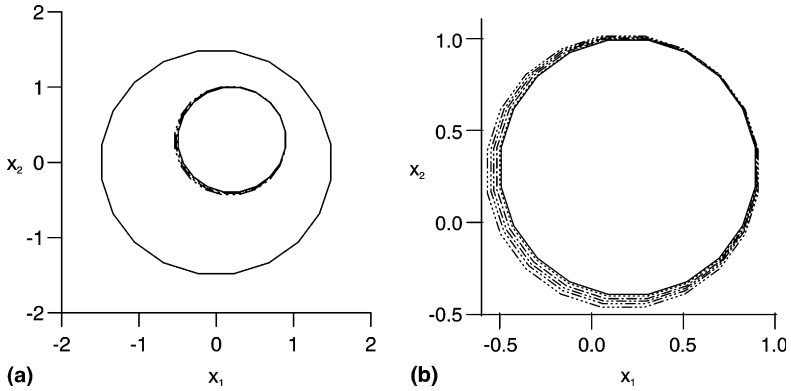

Fig. 3. (a) The exact (—) and the numerical solution for the cavity D_1 given by (E2), obtained with the initial guess (G2) and various levels of noise added into the temperature data $T|_{\partial\Omega}$, namely $p_T = 1\%$ (···), $p_T = 3\%$ (–·–), $p_T = 5\%$ (–··–), $p_T = 7\%$ (–···–) and $p_T = 10\%$ (–·····–), for Example 2 and (b) a closer view of the exact and numerical results obtained for the cavity D_1.

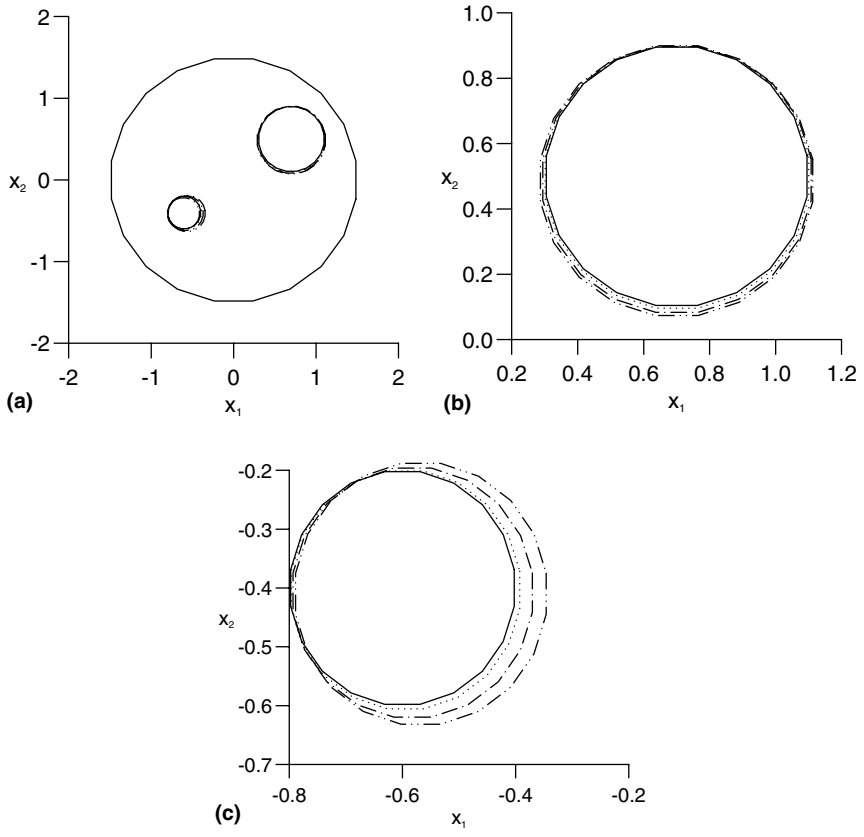

Fig. 4. (a) The exact (—) and the numerical solution for the cavities D_1 and D_2 given by (E3), obtained with the initial guesses (G3) and various levels of noise added into the temperature data $T|_{\partial\Omega}$, namely $p_T = 1\%$ (···), $p_T = 3\%$ (–·–) and $p_T = 5\%$ (–··–), for Example 3. A closer view of the exact and numerical results obtained for the cavities (b) D_1, and (c) D_2.

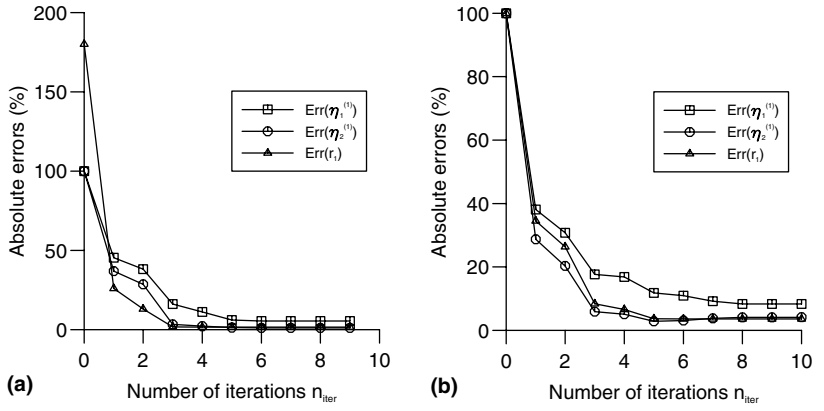

Fig. 5. The percentage absolute errors $\mathrm{Err}(\eta_1^{(1)})$ (–□–), $\mathrm{Err}(\eta_2^{(1)})$ (–○–) and $\mathrm{Err}(r_1)$ (–△–), as functions of the number of iterations n_{iter}, obtained with $p_T = 10\%$ noise added into the temperature data $T|_{\partial\Omega}$, and the initial guesses (G1) and (G2), for Examples (a) 1, and (b) 2, respectively.

5.3. Influence of the boundary conditions on the internal boundaries

For the inverse problem analysed in this paper it is impossible to obtain measurements on the boundaries of the cavities, since the location and size of the cavities embedded in the solution domain are not known. However, in practical engineering problems some boundary conditions are a priori known on the inner boundaries, in the sense that either the temperature distribution or the flux is prescribed on the boundaries of the cavities. Therefore, it is important to realise if and how much the type of boundary conditions given on the inner boundaries do influence the identification process. To do so, we consider Examples 1–3 and their corresponding exact solutions (E1)–(E3), respectively, and we try to retrieve the cavity/cavities using the same initial guess, the same amount of noise added into the outer boundary temperature or flux data and either temperature or flux data on the inner boundary, i.e. we solve both Problems 1 and 2 with the same initial guess and measurements on the outer boundary.

Fig. 6 presents the exact and the numerical solution for the cavity D_1 given by (E1), obtained for Example 1 starting with the initial guess (G1) and using noisy input temperature $\widetilde{T}|_{\partial\Omega}$, namely $p_T = 10$, and

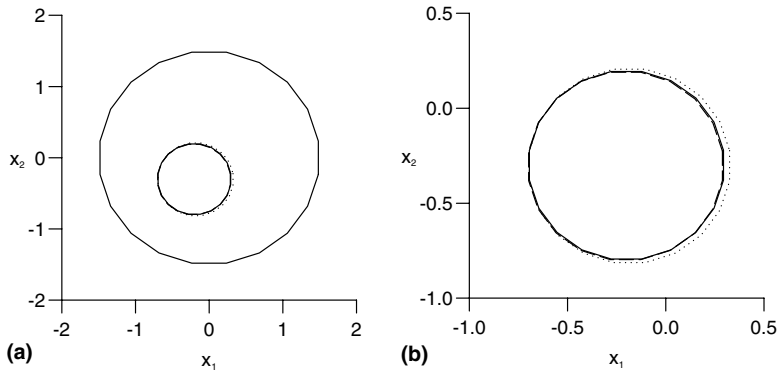

Fig. 6. (a) The exact (—) and the numerical solution for the cavity D_1 given by (E1), obtained with the initial guess (G1), $p_T = 10\%$ noise added into the temperature data $T|_{\partial\Omega}$, and temperature (···) and flux (––) measurements on $\partial\Omega_i$, for Example 1, and (b) a closer view of the exact and numerical results obtained for the cavity D_1.

different boundary conditions on the internal boundary. It can be seen that both numerical solutions for Problems 1 and 2 represent very good approximations for the exact cavity, with the mention that the cavity retrieved employing flux data on the inner boundary (Problem 2) is more accurate than that obtained using temperature data on the boundary of the cavity (Problem 1). Similar conclusions can be drawn from Figs. 7 and 8 which illustrate the numerical results obtained for the cavities D_j, $j = 1, \ldots, N_c$, in the case of Example 2 starting with the initial guess (G2) and $p_T = 10$ and Example 3 starting with the initial guess (G3) and $p_T = 5$, respectively, in comparison with their corresponding exact solutions. Moreover, from Figs. 6–8 it can be concluded that the cavity detection problem is more sensitive with respect to the type of inner boundary conditions for the modified Helmholtz equation than for the Helmholtz equation, in the sense that Neumann data on the inner boundaries provide more accurate approximate solutions. In addition, the influence of the boundary conditions on the inner boundaries is better emphasised in the case of identifying two cavities in Helmholtz-type equations, see e.g. Fig. 8.

5.4. Convergence of the method

Starting with the initial guess (G1) for the cavity D_1 and setting $p_T = 5$, we estimate the exact values (E1) using the numerical method proposed in Section 4, for the inverse problem given by Example 1. Fig. 9(a) illustrates the iterative convergence process as the initial guess for the cavity D_1 moves towards the target, for various numbers of iterations performed. From this figure it can be seen that the numerically retrieved cavity is a very good approximation of the target and the convergence is achieved after a small number of iterations, namely $n_{\text{iter}} = 9$. Consequently, the numerical results for the location and the size of the cavity, $\eta_1^{(1,\text{num})} = -0.1891$, $\eta_2^{(1,\text{num})} = -0.3035$ and $r_1^{(\text{num})} = 0.5079$ are in good agreement with their exact values. Fig. 9(b) presents the iterative convergence process for the numerical flux $\Phi^{(\text{num})}|_{\partial\Omega}$ towards its exact value $\Phi^{(\text{exact})}|_{\partial\Omega}$ for various numbers of iterations performed, namely $n \in \{1, 3, 6\}$, obtained for the inverse geometric problem given by Example 1. It can be seen that the convergence is very rapid and at the end of the iterative process the numerical and the exact values of the flux on the outer boundary $\partial\Omega$ are almost identical.

Similar results are obtained for the inverse problems given by Example 2 with the exact solution (E2), the initial guess (G2) and $p_T = 5$ and Example 3 with the exact solution (E3), the initial guess (G3) and $p_T = 3$, respectively. The iterative convergence process as the initial guess for the cavities D_j, $j = 1, \ldots, N_c$, where $N_c = 1$ in the case of Example 2 and $N_c = 2$ for Example 3, moves towards the target for the various num-

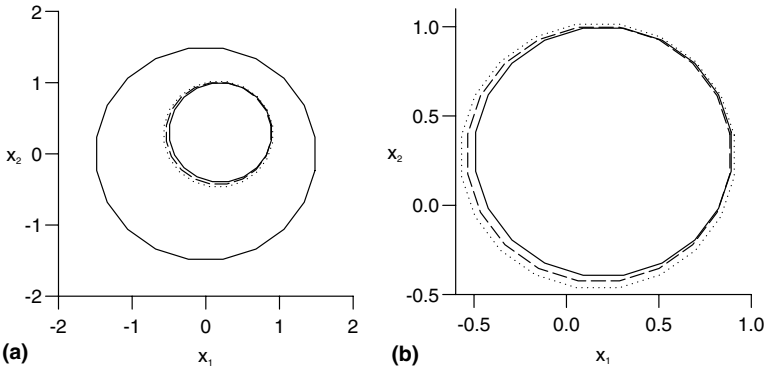

Fig. 7. (a) The exact (—) and the numerical solution for the cavity D_1 given by (E2), obtained with the initial guess (G2), $p_T = 10\%$ noise added into the temperature data $T|_{\partial\Omega}$, and temperature ($\cdots$) and flux (––) measurements on $\partial\Omega_i$, for Example 1, and (b) a closer view of the exact and numerical results obtained for the cavity D_1.

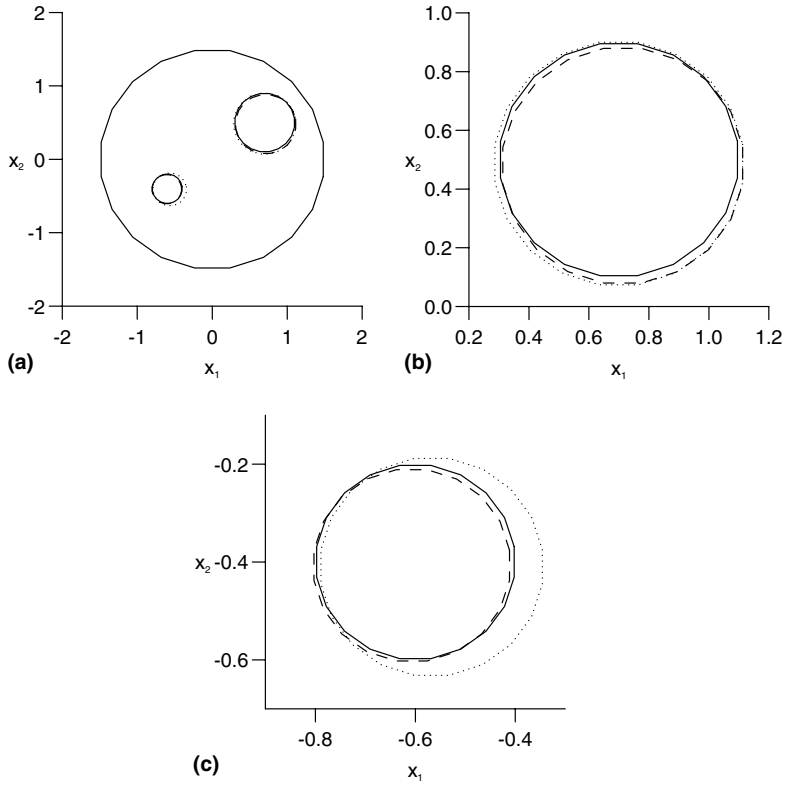

Fig. 8. (a) The exact (—) and the numerical solution for the cavities D_1 and D_2 given by (E3), obtained with the initial guesses (G3), $p_T = 5\%$ noise added into the temperature data $T|_{\partial\Omega}$, and temperature ($\cdots$) and flux ($--$) measurements on $\partial\Omega_i$, for Example 3. A closer view of the exact and numerical results obtained for the cavities (b) D_1, and (c) D_2.

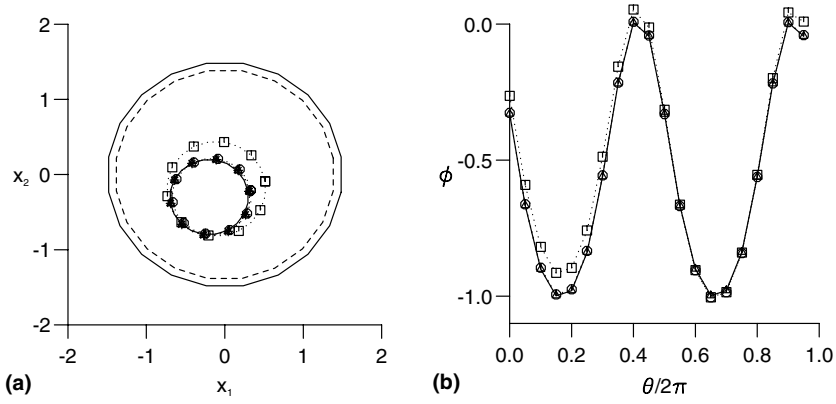

Fig. 9. The iterative convergence process for (a) the circular cavity D_1 as the initial guess (– – –) given by (G1) moves towards the target (—), i.e. the exact solution (E1), and (b) the numerical flux $\Phi^{(\mathrm{num})}|_{\partial\Omega}$ (—) towards the analytical flux $\Phi^{(\mathrm{an})}|_{\partial\Omega}$ (– – –), for $p_T = 5\%$ and various numbers of iterations performed, namely $n = 1$ ($\cdots\square\cdots$), $n = 3$ ($\cdots\bigcirc\cdots$), $n = 5$ ($\cdots\triangle\cdots$) and $n = 9$ ($\cdots*\cdots$), for Example 1.

bers of iterations performed are graphically presented in Fig. 10(a) and (b), respectively. It can be seen from these figures that the number of iterations n_{iter} required in order for the objective function $\mathscr{F}$ to attain

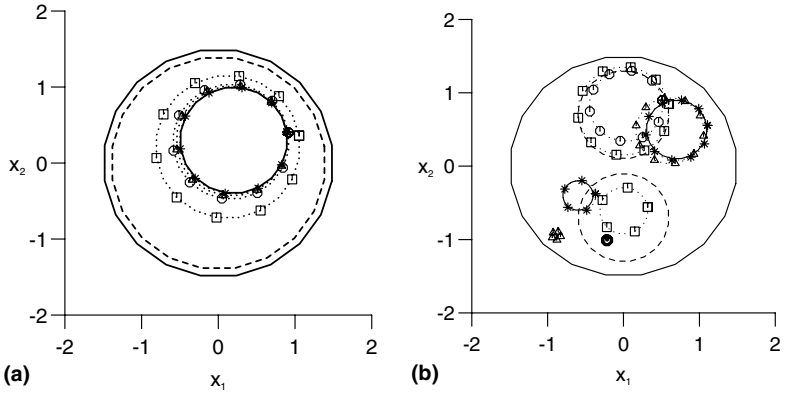

Fig. 10. (a) The iterative convergence process for the circular cavity D_1 as the initial guess (– – –) given by (G2) moves towards the target (—), i.e. the exact solution (E2), for $p_T = 5\%$ and various numbers of iterations performed, namely $n = 1$ ($\cdots\square\cdots$), $n = 3$ ($\cdots\bigcirc\cdots$), $n = 5$ ($\cdots\triangle\cdots$) and $n = 10$ ($\cdots *\cdots$), for Example 2. (b) The iterative convergence process for the circular cavities D_1 and D_2 as the initial guesses (– – –) given by (G3) move towards their targets (—), i.e. the exact solutions (E3), for $p_T = 3\%$ and various numbers of iterations performed, namely $n = 1$ ($\cdots\square\cdots$), $n = 5$ ($\cdots\bigcirc\cdots$), $n = 10$ ($\cdots\triangle\cdots$) and $n = 19$ ($\cdots *\cdots$), for Example 3.

convergence is larger in the case of Example 3 (i.e. $n_{\text{iter}} = 19$) than that obtained for Example 2 (i.e. $n_{\text{iter}} = 10$) and this is due to the larger number of cavity parameters involved in the minimisation function corresponding to Example 3. However, the number of iterations required to terminate the minimisation process is relatively small for all the inverse geometric problems investigated in this study.

5.5. Sensitivity analysis

Table 2 presents the numerical results obtained for the parameters characterising the position and the size of the cavity D_1 in comparison with their exact values corresponding to Example 2 with the initial guess (G2) and $p_T = 1$, when the position of the centre of the cavity is varied with respect to the x_1-coordinate $\eta_1^{(1)}$, while keeping the other parameters given by the exact solution (E2) constant, i.e. $\eta_2^{(1)} = 0.30$ and $r_1 = 0.70$. It can be seen that the numerical results retrieved using the numerical method proposed are very good approximations of their exact values, they are obtained after a maximum $n = 14$ iterations and the value of the objective function $\mathscr{F}$ is $O(10^{-4})$ in the worst case. From this table it can be seen that the numerical results obtained for the parameters determining the location and size of the cavity deteriorate as the bound-

Table 2
The values of the objective function $\mathscr{F}$, the number of iterations performed n_{iter} and the numerically retrieved values for the parameters characterising the position and the shape of the cavity D_1 given by $\eta_1^{(1)} \in \{0.10, 0.20, \ldots, 1.10\}$, $\eta_2^{(1)} = 0.30$ and $r_1 = 0.70$, obtained using $p_T = 1\%$ noise added into the input temperature data $T^{(\text{an})}|_{\partial\Omega}$ and the initial guess $\eta_1^{(1,\text{g})} = \eta_2^{(1,\text{g})} = 0.0$ and $r_1^{(\text{g})} = 1.40$, for Example 2

$\eta_1^{(1)}$	$\eta_1^{(1,\text{num})}$	$\text{Err}(\eta_1^{(1)})$	$\eta_2^{(1,\text{num})}$	$\text{Err}(\eta_2^{(1)})$	$r_1^{(\text{num})}$	$\text{Err}(r_1)$	$\mathscr{F}$	n_{iter}
0.00	0.0052	–	0.2927	2.4375	0.7053	0.7630	0.1821×10^{-3}	12
0.10	0.1002	0.2371	0.2952	1.5898	0.7055	0.7795	0.1606×10^{-5}	10
0.20	0.1974	1.3198	0.2968	1.0753	0.7054	0.7706	0.1640×10^{-5}	10
0.30	0.2975	0.8452	0.2968	1.0753	0.7051	0.7303	0.1998×10^{-5}	11
0.40	0.3962	0.9450	0.2979	0.6905	0.7046	0.6565	0.2714×10^{-5}	11
0.50	0.4894	2.1215	0.3024	0.7989	0.7040	0.5699	0.3535×10^{-5}	11
0.60	0.2747	54.2144	0.4905	63.4991	0.6968	0.4633	0.7509×10^{-3}	14

Table 3
The values of the objective function $\mathscr{F}$, the number of iterations performed n_{iter} and the numerically retrieved values for the parameters characterising the position and the shape of the cavities D_1 and D_2 given by $\eta_1^{(1)} = 0.70$, $\eta_2^{(1)} = 0.50$, $r_1 = 0.40$, $\eta_1^{(2)} = -0.50$, $\eta_2^{(2)} = -0.30$ and $r_2 \in \{0.10, 0.20, \ldots, 0.80\}$, obtained using $p_T = 1\%$ noise added into the input temperature data $T^{(\text{an})}|_{\partial\Omega}$ and the initial guess $\eta_1^{(1,\,\text{g})} = 0.0$, $\eta_2^{(1,\text{g})} = 0.70$, $r_1^{(\text{g})} = 0.60$, $\eta_1^{(2,\text{g})} = 0.0$, $\eta_2^{(2,\text{g})} = -0.70$ and $r_2^{(\text{g})} = 0.60$, for Example 3

r_2	$\eta_1^{(1,\text{num})}$ $\text{Err}(\eta_1^{(1)})$	$\eta_2^{(1,\text{num})}$ $\text{Err}(\eta_2^{(1)})$	$r_1^{(\text{num})}$ $\text{Err}(r_1)$	$\eta_1^{(2,\text{num})}$ $\text{Err}(\eta_1^{(2)})$	$\eta_2^{(2,\text{num})}$ $\text{Err}(\eta_2^{(2)})$	$r_2^{(\text{num})}$ $\text{Err}(r_2)$	$\mathscr{F}$	n_{iter}
0.10	0.7055	0.4917	0.4041	−0.5336	−0.3309	0.1016	0.3029×10^{-5}	24
	0.7832	1.6678	1.0149	6.7221	10.2919	1.6421		
0.20	0.7028	0.4961	0.4028	−0.4960	−0.3087	0.2053	0.5451×10^{-5}	25
	0.3934	0.7719	0.7716	0.7961	2.8860	2.6501		
0.40	0.6997	0.4985	0.4021	−0.4966	−0.3006	0.4029	0.4198×10^{-5}	14
	0.4092	0.2928	0.5349	0.6740	0.2134	0.7153		
0.50	0.6995	0.4989	0.4016	−0.4977	−0.3009	0.5024	0.3230×10^{-5}	14
	0.0715	0.2119	0.4018	0.4641	0.2902	0.4760		
0.60	0.6996	0.4992	0.4011	−0.4983	−0.3011	0.6021	0.2219×10^{-5}	13
	0.0612	0.1587	0.2682	0.3410	0.3741	0.3548		
0.70	0.6996	0.4994	0.4007	−0.4987	−0.3013	0.7020	0.1323×10^{-3}	16
	0.0612	0.1295	0.1635	0.2566	0.4239	0.2797		
0.80	0.5028	0.4219	0.2241	−0.4766	−0.3159	0.8274	0.3658×10^{-5}	22
	28.1726	15.6155	43.9713	4.6840	5.3146	3.4277		

ary of the cavity D_1 approaches the outer boundary of the domain Ω, i.e. for $\eta_1^{(1)} = 0.60$, $\eta_2^{(1)} = 0.30$ and $r_1 = 0.70$. Similar results have been obtained when varying $\eta_2^{(1)}$ and therefore they are not presented here.

In Table 3 we show the exact and the numerical results for the location and size of the cavities D_1 and D_2 corresponding to Example 3 with the initial guess (G3) and noisy input temperature data, i.e. $p_T = 1$ in (31), obtained using the BEM minimisation presented in Section 4, when the position and the size of the cavity D_1 and the location of the centre of the cavity D_2 given by the exact solution (E3) are kept constant, whilst the radius of the cavity D_2 is varied, namely $r_2 \in \{0.10, 0.20, \ldots, 0.80\}$. From this table it can be seen that better estimates of the parameters describing the position and the size of the cavity are obtained, provided that the radius, r_2, of the cavity is large. However, it should be noted that the numerical results obtained using the proposed numerical method deteriorate as the radius, r_2, of the cavity becomes very small, e.g. see the numerical results obtained for $r_2 = 0.10$, or the boundary of any of the cavities D_1 and D_2 approaches the outer boundary $\partial\Omega$, e.g. see the numerical results obtained when $r_2 = 0.80$, but they still represent reasonable estimates of their exact values. Although not presented here, it should be noted that the numerical results also deteriorate as the cavities D_1 and D_2 become very close.

It is worth noting that the algorithm proposed in this paper fails to provide reasonable results for large values of $|k|$ in the Helmholtz-type equation (1), i.e. $|k| \geqslant 4.0$, and the smaller the value of $|k|$, the more accurate are the numerical results. From Figs. 2–10 and Tables 1–3 it can be concluded that the numerical method described in Section 4 is very efficient in retrieving circular cavities of different sizes and locations embedded in the domain Ω, provided that noisy input data is available on the outer boundary of the domain under investigation.

6. Conclusions

In this paper, we have investigated the retrieval of circular cavities embedded in a two-dimensional domain where either the Helmholtz or the modified Helmholtz equation is satisfied, from boundary measurements only. It should be noted that the analysis performed in this study can be applied to other partial differential equations, such as convection–diffusion equations, which can be reduced to Eq. (1) with

$k \in \mathbb{R}$ or $k \in \mathbb{C} \setminus \mathbb{R}$, see e.g. [33]. The numerical method proposed combines a BEM presented in Section 3 and a constrained least-squares technique described in Section 4 in order to simultaneously identify the coordinates of the centres and the radii of the cavities.

From the numerical results presented and discussed in Section 5, it can be concluded that the proposed numerical method produces a stable numerical solution with respect to the location and the size of the circular cavities embedded in the two-dimensional domain Ω as the amount of noise added into the input temperature data on the outer boundary decreases. It was also found that the numerical results obtained for the parameters characterising the position and size of circular cavities deteriorate as the cavities become very small, the inhomogeneities are located in the vicinity of the outer boundary $\partial\Omega$ or the cavities are very close. However, even in these cases the numerical results obtained were found to have a reasonable accuracy. The very large values of $|k|$ for which the proposed numerical algorithm fails to provide accurate estimates of the cavities is another limitation of this method. However, future work will involve the numerical recovery of cavities in Helmholtz-type equations for large values of $|k|$, as well as the detection of other shapes, such as polygons or ellipses.

Acknowledgement

The author would like to thank Dr. Daniel Lesnic from the Department of Applied Mathematics, at the University of Leeds, for the fruitful discussions and all his encouragement in performing this research work.

References

[1] S. Kubo, Inverse problems related to the mechanics and fracture of solids and structures, JSME Int. J. 31 (1988) 157–166.
[2] J. Hadamard, Lectures on Cauchy Problem in Linear Partial Differential Equations, Oxford University Press, London, 1923.
[3] J.V. Beck, B. Blackwell, C.R. St. Clair, Inverse Heat Conduction: Ill-Posed Problems, Wiley-Interscience, New York, 1985.
[4] D. Colton, R. Kress, Inverse Acoustic and Electromagnetic Scattering, Springer Verlag, Berlin, 1992.
[5] M. Ikehata, Enclosing a polygonal cavity in a two-dimensional bounded domain from Cauchy data, Inv. Prob. 15 (1999) 1231–1241.
[6] M. Ikehata, T. Ohe, A numerical method for finding the convex hull of polygonal cavities using the enclosure method, Inv. Prob. 18 (2002) 111–124.
[7] M. Tanaka, Y. Masuda, Boundary element method applied to some inverse problems, Engrg. Anal. 3 (1986) 138–143.
[8] M. Tanaka, M. Nakamura, T. Nakano, Defect shape identification by the elastodynamic boundary element method using strain responses, in: M. Tanaka, C.A. Brebbia, R. Shaw (Eds.), Advances in BEM in Japan and USA, CMP, Southampton, UK, 1990, pp. 137–151.
[9] M. Tanaka, M. Nakamura, T. Nakano, Defect shape identification by boundary element method combined with method of multiple force applications, in: M. Tanaka, Q. Du (Eds.), Boundary Element Methods: Principles and Applications, Pergamon Press, Oxford, UK, 1990, pp. 319–328.
[10] L.M. Bezerra, S. Saigal, A boundary element formulation for the inverse elastostatics problem (IESP) of flaw detection, Int. J. Numer. Meth. Engrg. 36 (1993) 2189–2202.
[11] S.C. Mellings, M.H. Aliabadi, Flaw identification using the boundary element method, Int. J. Numer. Meth. Engrg. 38 (1995) 399–419.
[12] A.J. Kassab, F.A. Moslehy, A.B. Daryapurkar, Nondestructive detection of cavities by an inverse elastostatics boundary element method, Engrg. Anal. Bound. Elements 13 (1994) 45–55.
[13] T.W. Ulrich, F.A. Moslehy, A.J. Kassab, A BEM based pattern search solution for a class of inverse elastostatic problems, Int. J. Solids Struct. 33 (1996) 2123–2131.
[14] V. Mallardo, M.H. Aliabadi, A BEM sensitivity and shape identification analysis for acoustic scattering in fluid–solid problems, Int. J. Numer. Meth. Engrg. 41 (1998) 1527–1541.
[15] G. Rus, R. Gallego, Optimization algorithms for identification inverse problems with the boundary element method, Engrg. Anal. Bound. Elements 26 (2002) 315–327.
[16] R. Gallego, G. Rus, Identification of cracks and cavities using the topological boundary integral equation, Comput. Mech. 33 (2004) 154–163.

[17] L. Marin, L. Elliott, D.B. Ingham, D. Lesnic, Identification of material properties and cavities in two-dimensional linear elasticity, Comput. Mech. 31 (2003) 293–300.
[18] E.A. Divo, A.J. Kassab, F. Rodriguez, An efficient singular superposition technique for cavity detection and shape optimization, in: M. Tanaka (Ed.), Inverse Problems in Engineering Mechanics V, Nagano, Japan, 2003, pp. 241–250.
[19] A.J. Kassab, E.A. Divo, A. Hadjinicolaou, A hybrid BEM/singular superposition algorithm to solve the inverse geometric problem applied to subsurface cavity detection, in: M. Tanaka, C.A. Brebbia, R. Shaw (Eds.), Inverse Problems, Design and Optimization Symposium, Rio de Janeiro, Brazil, 2004.
[20] D.E. Beskos, Boundary element method in dynamic analysis: Part II (1986–1996), ASME Appl. Mech. Rev. 50 (1997) 149–197.
[21] J.T. Chen, F.C. Wong, Dual formulation of multiple reciprocity method for the acoustic mode of a cavity with a thin partition, J. Sound Vib. 217 (1998) 75–95.
[22] I. Harari, P.E. Barbone, M. Slavutin, R. Shalom, Boundary infinite elements for the Helmholtz equation in exterior domains, Int. J. Numer. Meth. Engrg. 41 (1998) 1105–1131.
[23] W.S. Hall, X.Q. Mao, A boundary element investigation of irregular frequencies in electromagnetic scattering, Engrg. Anal. Boundary Elem. 16 (1995) 245–252.
[24] P.P. Goswami, T.J. Rudophi, F.J. Rizzo, D.J. Shippy, A boundary element model for acoustic interaction with applications in ultrasonic NDE, J. Nondestr. Eval. 9 (1990) 101–112.
[25] A.D. Kraus, A. Aziz, J. Welty, Extended Surface Heat Transfer, John Wiley & Sons, New York, 2001.
[26] O.D. Kellogg, Foundations of Potential Theory, New Haven, Dover, 1923.
[27] S. Kim, M. Yamamoto, Uniqueness in the two-dimensional inverse conductivity problems in determining convex polygonal supports: case of variable conductivity, Inv. Prob. 20 (2004) 495–506.
[28] A. Morassi, E. Rosset, Stable determination of cavities in elastic bodies, Inv. Prob. 20 (2004) 453–480.
[29] G. Chen, J. Zhou, Boundary Element Methods, Academic Press, London, 1992.
[30] L. Marin, L. Elliott, P.J. Heggs, D.B. Ingham, D. Lesnic, X. Wen, An alternating iterative algorithm for the Cauchy problem associated to the Helmholtz equation, Comput. Methods Appl. Mech. Engrg. 192 (2003) 709–722.
[31] L. Marin, L. Elliott, P.J. Heggs, D.B. Ingham, D. Lesnic, X. Wen, Conjugate gradient-boundary element solution to the Cauchy problem for Helmholtz-type equations, Comput. Mech. 31 (2003) 367–377.
[32] P.E. Gill, W. Murray, M.H. Wright, Practical Optimization, Academic Press, London, 1981.
[33] K. Chen, Improving the accuracy of DRBEM for convective partial differential equations, Engrg. Anal. Bound. Elements 23 (1999) 639–644.